# Benchmarks and reliable DFT results for spin-crossover complexes

Suhwan Song, Min-Cheol Kim, and Eunji Sim
*Department of Chemistry, Yonsei University, 50 Yonsei-ro Seodaemun-gu, Seoul 03722, Korea*

Anouar Benali
*Argonne Leadership Computing Facility, Argonne National Laboratory, 9700 S. Cass Ave, Argonne, IL 60439, USA*

Olle Heinonen
*Material Science Division, Argonne National Laboratory, 9700 S. Cass Ave, Argonne, IL 60439, USA*

Kieron Burke
*Departments of Chemistry and of Physics, University of California, Irvine, CA 92697, USA*
(Dated: Monday 28th August, 2017)

DFT is used throughout nanoscience, especially when modeling spin-dependent properties that are important in spintronics. But standard quantum chemical methods (both CCSD(T) and self-consistent semilocal density functional calculations) fail badly for the spin adiabatic energy difference in Fe(II) spin-crossover complexes. We show that all-electron fixed-node diffusion Monte Carlo can be converged at significant computational cost, and that the B3LYP single-determinant has sufficiently accurate nodes, providing benchmarks for these systems. We also find that density-corrected DFT, using Hartree-Fock densities (HF-DFT), greatly improves accuracy and reduces dependence on approximations for these calculations. The small gap in the self-consistent DFT calculations for the high-spin state is consistent with this. For the spin adiabatic energy differences in these complexes, HF-DFT is both accurate and reliable, and we make a strong prediction for the Fe-Porphyrin complex. The "parameter-dilemma" of needing different amounts of mixing for different properties is eliminated by HF-DFT.

Density Functional Theory (DFT) calculations are used throughout nanoscience,[1–6] but their primary purpose is to yield accurate relative energetics and geometries.[7, 8] Spin and magnetic properties are also ubiquitous, but the reliability of magnetic moments and other spin-dependent properties from DFT is far less well-established.[9–12] In the case of molecular transport, the well-known inaccuracies of DFT orbital energies have been linked to the typical overestimate of calculated conductances.[13–16] Thus spintronics DFT calculations have numerous sources of uncertainty,[17] but for many applications, only DFT calculations are feasible.[18]

Spin-crossover complexes (SCO) provide an ideal setting for examining the reliability of DFT for spin-dependent properties.[19] These have been modeled in spintronics studies, both for the isolated molecule and coupled to the leads.[20–24] The energy difference between the high- (HS) and low-spin (LS) states is relatively small, and their spin-state can be flipped by entropic effects, even at room temperature.[25–27] Because it is very difficult to isolate such complexes experimentally,[28, 29] DFT calculations must be benchmarked against high-accuracy quantum chemical calculations. If DFT is unable to predict the lowest energy spin-state accurately, spintronic calculations will certainly fail.

Here we carefully analyze DFT calculations of the spin adiabatic energy difference (SA), $E^{SA} = E_{HS} - E_{LS}$, of four well-studied SCOs.[30–33] These SAs are all within a few eV, due to $d$-type orbitals being close in energy. Standard DFT calculations give surprisingly large variations, including predicting the incorrect ground state. *Ab initio* calculations, including CCSD(T), are notoriously difficult and fickle for such SCO systems.[12, 34] Many of the central results of the current work are illustrated in Fig. 1. The horizontal dashed lines are extremely expensive but converged diffusion Monte Carlo (DMC) results, showing the errors in large-basis CCSD(T) calculations which are represented as dot-dashed line. Red points show approximate DFT results, ranging from Localized Density Approximation (LDA) on the left to PBE0 on the right, with increasing fraction of Hartree Fock (HF) exchange, and decreasing $E^{\rm SA}$. In particular, the CO ligand results have the largest spread, about 4 eV. The highly accurate DMC results show that the DFT results all overstabilize the LS state relative to HS. The hybrids do best,[32, 35, 36] as SA decreases with increasing fraction of exact exchange portion. But we also include the blue points, which are the results from the various DFT approximations evaluated on HF densities, (HF-DFT) a simple procedure suggested by the theory of density-corrected DFT (DC-DFT).[37–41] The figures clearly show that HF-DFT is both much more accurate and has much less variation than standard self-consistent DFT. The rest of this paper explains how this can be.

Begin with *ab initio* calculations, CCSD and CCSD(T) on a TZVP basis yielded seemingly reasonable results, running about one day on a moderate cluster. But they have two important flaws. When a cc-pVTZ basis was used instead, requiring about a week to run, the results shift by up to 1.0 eV, showing that even this basis is insufficient. Moreover D1, a diagnostic available in Turbomole[42], is above 0.04 for all cases, whereas perturbative triples are only reliable when D1 is order 0.02 or less,[43] suggesting neither CCSD

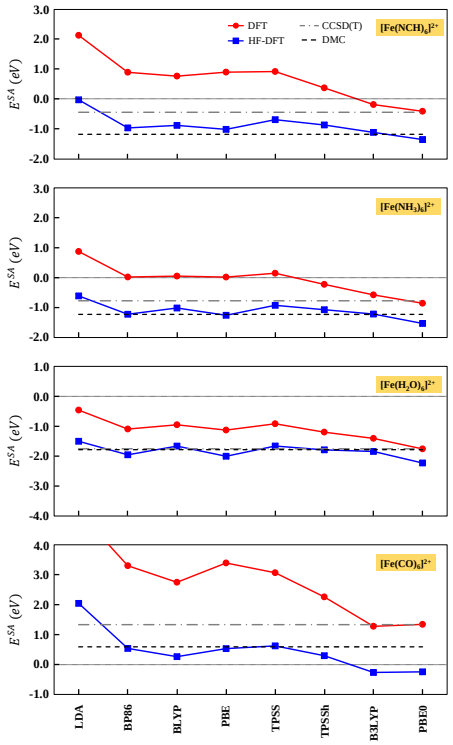


FIG. 1. Spin adiabatic energy differences of Fe(II) complexes for various DFT calculations and CCSD(T) (gray, unconverged) and diffusion Monte Carlo (black).

nor CCSD(T) is reliable for these problems.[44] (See Table S14 of the supporting information).

What to do? In recent decades, Quantum Monte Carlo (QMC) methods, and particularly fixed-node diffusion Monte Carlo, (FN-DMC)[45] have proven successful at accurately describing the properties of many solids [45–50] and molecules.[51–57] In DMC we minimize the expectation value of the many-body Hamiltonian when propagating a convolution of the many-body wavefunction with the Green's function in imaginary time using many random walkers. In the fixed node (FN) approximation, the positive and negative regions of an initial trial wavefunction are maintained and the walkers, which sample electrons' positions, do not cross nodal lines. The accuracy of the wavefunction and the obtained upper bound for the ground state energy are limited by the quality of the nodal surface of the trial wavefunction. A trial wavefunction ($\Psi_T$) is often the product of a determinant of orbitals ($\Psi_{AS}$) (fixing the nodes) and a Jastrow function whose parameters are found by minimizing the energy through an initial variational MC scheme. The accuracy of the FN-DMC wavefunction depends solely on the quality of the nodal surface of $\Psi_{AS}$, whose orbitals are usually taken from an effective single-particle theory, such as HF or DFT. Single-determinant FN-DMC yields errors below 1 kcal/mol for van der Waals molecules[52–54], transition metal molecules[58, 59] and strongly correlated solids.[47–49, 60–63] Moreover, any such DMC result can be systematically improved by increasing the complexity of $\Psi_{AS}$ by including more determinants. Essentially exact results for the $H_2O$ molecule[64] were obtained from a selected Configuration Interaction method, and for the G1 test set[57] using a Complete Active-Space Self-Consistent Field construct, and is showing promising results for solids.[65] QMC also has only a weak dependence on the basis set[57, 66] and costs scale as $N^3$ with the number of electrons $N$, allowing the study of large systems, as the FN-DMC algorithm can efficiently use millions of processors, including both CPUs and GPUs[67–69].

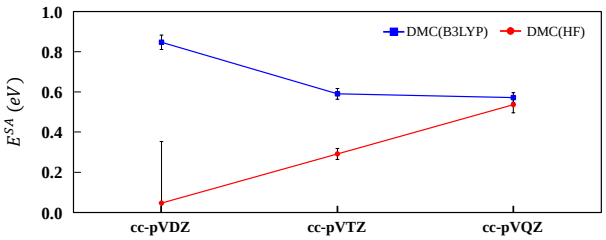


FIG. 2. SA of $[Fe(CO)_6]^{2+}$ evaluated with DMC with two different trial Slater determinants and three different basis sets.

As pseudopotentials for Fe can hold large locality errors in DMC[70], we perform all-electron DMC. We use a single-determinant B3LYP trial wavefunction for our DMC calculations, and use cc-pVNZ basis sets, where N=D,T,Q. We use the most challengling case, CO, to test convergence. We used a time step of 0.005 and 32k walkers. To reduce the variance we used 1-, 2- and 3-body Jastrow functions applied on all atoms and optimized for each individual spin state. For the largest basis sets, (cc-pVTZ and cc-pVQZ), we used 200k-400k core hours on 512 Intel Knight's Landing nodes to reach a DMC accuracy of about 25meV per compound. Figure 2 shows that when using a *single-determinant* B3LYP trial wavefunction, SA energies converge within 20 $\pm$ 20 meV with the size of the basis-set, and are already converged at the cc-pVTZ level. The HF reference recovers the same result, but requires the larger basis set.

Despite the failure of CCSD(T), a single Slater determinant provides sufficiently accurate nodes for DMC. Thus a system having multireference character in traditional quantum chemical language does not necessarily imply a nodal surface that requires more than one Slater determinant. The 2- and 3-body Jastrow factors account for considerable correlation. This is consistent with claims of the weak dependence on basis-sets size in QMC. For all remaining compounds, we chose to carry all calculations with all electrons, a cc-pVTZ basis set, a B3LYP trial wavefunction and spin-compound optimized 1-3 Body Jastrows.

In contrast with quantum chemical methods, DFT calculations converge more rapidly with basis set. All calculations here were done in cc-pVTZ and many were compared with the Fritz Haber Institute molecular simulations package (FHI-aims), yielding agreement to within 0.01 eV in all cases. (See Table S2 in the supporting Information.) We

next explain the difference between the red and blue lines in Fig. 1.

Ground-state Kohn-Sham (KS) DFT is mostly used to extract approximate ground-state energies of electronic systems as a function of nuclear positions.[71] But every practical calculation uses an approximation to the unknown exchange-correlation (XC) energy, and the self-consistent cycle of a KS solver finds the density that minimizes the approximate energy for the given system.[72] Thus both the density and energy are approximated.[38] It is trivial to separate out the energetic consequences of these two approximations. The energy error in such a calculation may be defined as

$$\Delta E = \tilde{E}[\tilde{n}] - E[n], \tag{1}$$

where the tilde indicates the approximation. We define the functional ($\Delta E_F$) and density-driven ($\Delta E_D$) errors as[38]

$$\Delta E_F = \tilde{E}[n] - E[n], \quad \Delta E_D = \tilde{E}[\tilde{n}] - \tilde{E}[n], \tag{2}$$

so they sum to the total energy error. For a KS calculation, $\Delta E_F = \Delta \tilde{E}_{xc}[n]$, the error in the approximation to exchange-correlation, while $\Delta E_D \leq 0$ by the variational principle. In normal KS-DFT calculations, the density is so good that $|\Delta E_D| << \Delta E_F$. But semilocal and hybrid functionals suffer from self-interaction (or delocalization) error.[73] In many cases, this error is density-driven, and $|\Delta E_D|$ becomes comparable to $\Delta E_F$. We call such calculations *abnormal*, and the error can be significantly reduced by using a more accurate density. For atoms and molecules, the HF density is often sufficient, so that HF-DFT yields much better results. This has been shown to reduce errors for anions,[37] transition state barriers,[74] ions and radicals in solution,[39] and dissociating heterogeneous diatomics,[40] as discussed in a recent review.[41]

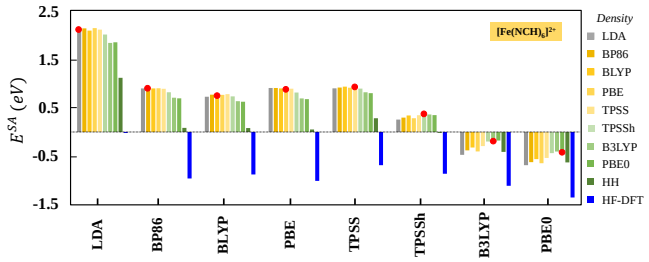


FIG. 3. Spin adiabatic energy difference of $[Fe(NCH)_6]^{2+}$ evaluated with different DFT approximations on several different self-consistent (red dots) and HF (blue) densities. ( Dark green bar is the self-consistent density of Becke's half-and-half functional (HH), with 50% exact exchange.)

To demonstrate sensitivity to the density, in Fig. 3 we show SA for several different approximations on different densities. We consider here simple, commonly-used DFT approximations. LDA uses only the density at a point, generalized gradient approximations (GGAs) use both the density and its gradient, while (global) hybrids mix some exact exchange with GGA[75]:

$$E_{xc}^{hyb}[n] = E_{xc}^{GGA}[n] + a(E_x^{HF}[n] - E_x^{GGA}[n]), \tag{3}$$

where $a$ is the amount of exchange mixing. In addition, we include metaGGAs (mGGAs), which also depend on a local kinetic energy density, in the generic term GGA. In practice, all approximations are spin-density functionals, so $n(\mathbf{r})$ represents spin-densities here. For a given energy approximation, there is little difference between evaluation on LDA, GGA or mGGA densities. However, the result changes with the amount of exchange mixing. TPSSh has 10% and B3LYP and PBE0 have 20% and 25%, respectively, while Becke's half-and-half (HH) has 50%. The SA decreases with increasing $a$ in the density and even becomes correctly negative with a HF density (100% exact exchange). Similar results are found for all four complexes. The strong dependence on $a$ for the density demonstrates that these DFT calculations are *abnormal*, i.e., a significant fraction of the error in such calculations is density-driven. We recommend the use of such 2D *rainbow* plots, Fig. 3, as a check for density-driven errors, as they do not require knowledge of the accurate result.

Knowing that there is a strong-density-driven error does not guarantee that a HF density is sufficiently close to the exact density to improve the DFT results, but Fig. 1 strongly suggests that this is the case here. Table I reports the errors in that figure. (Results of cc-pVTZ can be found in Tables S1-S4 of the supporting information and Tables S11 and S12 are those of TZVP.) The first few rows show the results of *ab initio* quantum chemical methods. HF is very poor, with typical errors of about 3 eV. CCSD does much better, but inclusion of perturbative triples doubles the errors, unlike in main-group chemistry, suggesting a multi-reference nature, corroborated by the high D1 values. To check the reliability of our DMC with just a single Slater determinant trial wavefunction, for the CO complex, we constructed a multi-determinant trial wavefunction consisting of 135 k determinants using the perturbatively selected configuration interaction method (CIPSI) as described in Ref. 76. In order to make the calculation tractable, and only for this test, we used a pseudopotential for the Fe atom. We compared the variational energies from this multideterminant expansion with the energies obtained from DMC with the B3LYP nodal surface using the same pseudopotential and basis set. The calculations yielded the same $E^{SA}$ to within a $\pm 0.005$ a.u. error bar. More details of this calculation will appear elsewhere.

Another signal that a self-consistent DFT calculation might suffer from a density-driven error is an abnormally small HOMO-LUMO gap, often less than 1 eV.[38] The gaps for all molecules and functionals are listed in the supporting Information, talbe S10, for both HS and LS states. For the HS states, all gaps are below 1 eV, with some as small as 0.4 eV.

In self-consistent DFT, typical LDA errors are similar in magnitude but opposite in sign to those of HF. All DFT approximations overstabilize the LS state relative to the HS state in a very systematic way. Typical GGAs are about 1.7

TABLE I. Errors in SA in eV relative to DMC. Note that DMC values in eV are -1.17 for NCH, -1.23 for $NH_3$, -1.78 for $H_2O$ and 0.59 for CO. The column MAE is mean absolute errors over all 4 molecules. Rows AVG average over all GGA and hybrid energies, while RMSD gives their root-mean square deviation.

| Method | NCH | $NH_3$ | $H_2O$ | CO | MAE |
|---|---|---|---|---|---|
| **Ab initio** | | | | | |
| HF | -2.45 | -2.04 | -1.79 | -5.24 | 2.88 |
| CCSD | 0.28 | 0.13 | -0.19 | -0.20 | 0.20 |
| CCSD(T) | 0.74 | 0.45 | 0.03 | 0.74 | 0.49 |
| **SC-DFT** | | | | | |
| SVWN | 3.31 | 2.10 | 1.32 | 4.51 | 2.81 |
| *GGA* | | | | | |
| BP86 | 2.07 | 1.25 | 0.69 | 2.71 | 1.68 |
| BLYP | 1.94 | 1.28 | 0.83 | 2.16 | 1.55 |
| PBE | 2.08 | 1.25 | 0.65 | 2.80 | 1.69 |
| TPSS | 2.10 | 1.37 | 0.86 | 2.48 | 1.70 |
| *Hybrid* | | | | | |
| TPSSh | 1.55 | 1.00 | 0.58 | 1.67 | 1.20 |
| B3LYP | 1.00 | 0.65 | 0.37 | 0.68 | 0.68 |
| PBE0 | 0.77 | 0.37 | 0.02 | 0.75 | 0.48 |
| AVG | 1.64 | 1.02 | 0.57 | 1.89 | 1.28 |
| RMSD | 0.52 | 0.35 | 0.27 | 0.82 | 0.49 |
| **HF-DFT** | | | | | |
| SVWN | 1.15 | 0.62 | 0.28 | 1.45 | 0.88 |
| *GGA* | | | | | |
| BP86 | 0.21 | 0.00 | -0.17 | -0.05 | 0.11 |
| BLYP | 0.30 | 0.21 | 0.12 | -0.33 | 0.24 |
| PBE | 0.17 | -0.03 | -0.22 | -0.06 | 0.12 |
| TPSS | 0.49 | 0.30 | 0.12 | 0.03 | 0.24 |
| *Hybrid* | | | | | |
| TPSSh | 0.31 | 0.15 | -0.01 | -0.30 | 0.19 |
| B3LYP | 0.07 | 0.01 | -0.06 | -0.86 | 0.25 |
| PBE0 | -0.17 | -0.30 | -0.45 | -0.84 | 0.44 |
| AVG | 0.25 | 0.15 | 0.16 | 0.35 | 0.23 |
| RMSD | 0.19 | 0.18 | 0.19 | 0.34 | 0.23 |

eV too high. The best functional is the hybrid PBE0 with a mean absolute error of 0.5 eV, and the performance of other hybrids depend on the amount of mixing. Averaging over all 4 GGAs and 3 hybrids yields 1.3 eV error, and the root-mean-square deviation (RMSD) from this value is about 0.5 eV. But when evaluated on HF densities, the typical LDA error is reduced by a factor of 3, while GGA errors are below 0.25 eV and are now comparable to hybrids. The average HF-DFT error is now within 0.25 eV, with RMSD deviations of 0.23 eV. Clearly, both the accuracy of the typical functional is substantially higher, and the variations among functionals much lower than in self-consistent DFT. Moreover, the most accurate results are from either BP86 or PBE, both simple GGAs, with no exchange mixing. BP86 was previously identified as (at the time of testing) the most accurate for transition metal complexes.[35] Thus HF-DFT yields much more reliable and accurate estimates of SA for these molecules.

To relate density differences to density-driven errors, we focus on LS $[Fe(CO)_6]^{2+}$ as an example, comparing densities using DMC with the GAMESS B3LYP all electron trial wavefunction with PBE and HF densities obtained with FHI-aims. The left panel of Fig. 4 shows isosurfaces of the HF and PBE electron number density difference at $\pm 0.1$ Å$^{-3}$, with gold (blue) positive (negative) values. The HF density polarizes the oxygen more, shifting density towards the Fe ion at the center. This is visible as gold (positive density difference) regions closer to the Fe ion. Also, the PBE density shows much more pronounced lobes from the $3d_{z^2}$ and the $3d_{x^2-y^2}$ orbitals, visible as blue (negative density difference) lobes near the center. The middle panel shows the DMC and PBE density difference. This is *qualitatively* similar to the HF and PBE density difference in that the oxygen is more polarized in DMC than PBE, and also by the less pronounced $3d$ orbital lobes at Fe ion (visible as dimples with blue centers in the gold cuboid). Finally, the right panel shows the DMC and HF density difference. This figure shows that DMC polarizes the oxygen more than does HF, and also that the Fe $3d$ lobes are somewhat more extended in DMC than HF. We speculate that the key reason the HF-DFT scheme yields quantitatively more accurate energies than DFT is that the HF Fe $3d$ lobes, like in DMC, are less pronounced than in DFT.

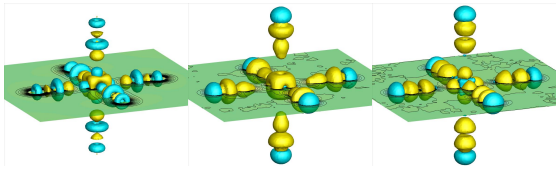

FIG. 4. Isosurface plots of difference densities at $\pm 0.1$ Å$^{-3}$ for the LS $[Fe(CO)_6]^{2+}$ complex, with gold (blue) +0.1 (-0.1) Å$^{-3}$. Left panel: $n^{HF} - n^{PBE}$. Middle panel: $n^{DMC} - n^{PBE}$. Right panel: $n^{DMC} - n^{HF}$.

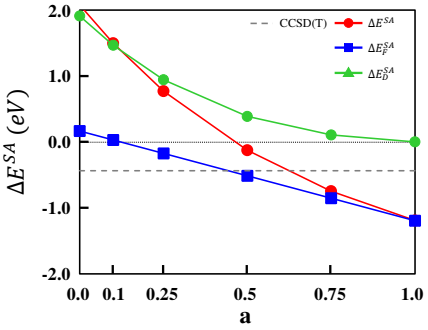


FIG. 5. Error in spin adiabatic energy difference of $[Fe(NCH)_6]^{2+}$ complex from $a$PBE, decomposed into functional and density-driven components.

Now, we analyze the effect of the exchange mixing parameter $a$ for NCH, assuming that the HF density is exact. To do this, we run both self-consistent and HF-DFT calculations for $a$PBE, which is the PBE functional with a variable fraction $a$ of exact exchange. If we assume that the self-consistent density of 1.0PBE (i.e., 100% exact exchange) is negligibly different from the exact density, all compo-

nents are easy to calculate within HF-DFT, and are plotted in Fig. 5. The functional error is almost perfectly linear, reflecting the linear dependence on the exact exchange energy. The density-driven error vanishes for $a = 1$, based on our assumptions. The plot shows that, for the pure GGA ($a = 0$), the error is almost entirely density-driven. Turning on $a$ reduces the density-driven error, but increases the functional error (the parameter dilemma). For some intermediate value of $a$, here about 0.45, the two contributions cancel, but there's no reason that this amount of mixing won't change from molecule to molecule. The parameter dilemma most often arises when the position of the HOMO or the size of the gap is important for some property or prediction. Then often increasing $a$ improves the positions of the orbitals or the gap, but worsens the underlying energetics. HF-DFT avoids this Procrustean dilemma, as the HF density is typically very similar to a KS calculation with the exact exchange, whose potential has excellent orbital properties.

Lastly, we show DFT calculations on the Fe-Porphyrin complex. This is too large to perform either CCSD(T) or DMC in the basis sets used throughout this paper. But Fig. 6 shows the results of self-consistent and HF-DFT calculations. Fig. 6 clearly demonstrates the tremendous reduction in variation among approximate energies when the HF density is consistently used, and the unambiguous prediction that the LS state is lower by about 0.8 eV, in contradiction to self-consistent B3LYP or PBE0. Fe(P)NO complex is known to be strongly correlated[34] and, furthermore, requires a multi-reference treatment for accurate description.[77, 78] Nevertheless, HF-DFT successfully eliminates the chronic problem of its variational counterpart, the functional dependency.

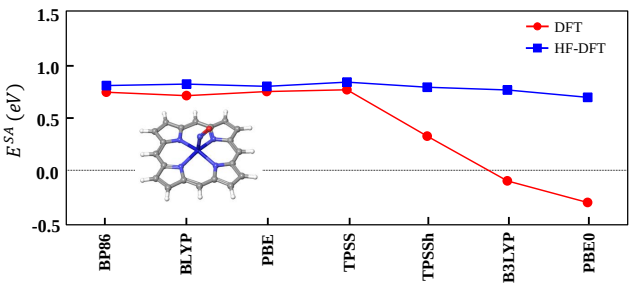


FIG. 6. Spin adiabatic energy difference of Fe(P)NO where P denotes porphyrin.

We have shown that standard quantum chemical methods fail for the SA of Fe(II) SCOs. Semilocal DFT calculations give wildly different results and suffer from the parameter dilemma, while even with a decent basis set, CCSD(T) calculations are both unconverged and unreliable. But extremely demanding DMC methods can be converged to provide benchmarks for these systems. All-electron calculations using up to 3-body Jastrow factors converge in cc-pVQZ. Surprisingly, the B3LYP single Slater determinant is a sufficiently accurate trial wavefunction, and converges more rapidly than the HF wavefunction.

We have also shown that HF-DFT yields much better results (errors reduced by a factor of 3 or more) for these calculations, and do not suffer from a parameter dilemma. This is because these calculations are *abnormal*[41]: Semilocal DFT calculations of the SA of these compounds are contaminated by density-driven errors. Their small HOMO-LUMO gap for the HS state is consistent with this hypothesis. In such cases, and when a HF calculation does not suffer from spin-contamination, often using a HF density greatly reduces the DFT error, as is the case here. This does not mean that the HF density is generally 'better' than the self-consistent DFT density. It simply means that the semilocal DFT SA is more accurate on the HF density, as it does not suffer from the delocalization error in the density of semilocal DFT. This is a property of the type of DFT approximation, the specific energy calculated, and the specific system under study[41]. We caution against overgeneralization of these results.

## 1. METHODS

All HF, CCSD(T) and DFT calculations presented in Figs. 1 and 3 as well as in Table I were carried out with TURBOMOLE v7.0.2[42] and LDA (SVWN5), GGA (PBE, BP86, BLYP), mGGA (TPSS), and hybrid (TPSSh, B3LYP, PBE0) functionals were used for the DFT and HF-DFT calculations. The scripts for performing HF-DFT energy calculations are available.[79] The geometries used were B3LYP with TZVP basis set. Geometry information can be found in Tables S5-S8 of the supporting information. We also performed fixed-spin HF and DFT calculations using FHI-aims 160328_3.[80] All FN-DMC (QMC) calculations used the QMCPACK code[67–69]. Relativistic corrections were ignored as Fe is rather light and relativistic effects are usually not important. Adding zero order scalar relativistic corrections within FHI-aims (control keywords "relativistic atomic zora") for CO and $H_2O$ changed the $E_{SA}$ results by at most 0.2 eV, worsening agreement with DMC.

## ACKNOWLEDGEMENTS

This work at Yonsei University (2016-22-0121) was supported by the grants from the Korean Research Foundation (2017R1A2B2003552, 2014R1A1A3049671) and the Ministry of Trade, Industry & Energy, Rep. of Korea (No.10062161). K.B. acknowledges DOE grant DE-FG02-08ER46496. AB and OH were supported by the U.S. Department of Energy, Office of Science, Basic Energy Sciences, Materials Sciences and Engineering Division, as part of the Computational Materials Sciences Program and Center for Predictive Simulation of Functional Materials. Diffusion Monte Carlo calculations were carried through an award of computer time provided by the Innovative and Novel Computational Impact on Theory and Experiment (INCITE) program. This research has used resources of the Argonne

Leadership Computing Facility, which is a DOE Office of Science User Facility supported under Contract DE-AC02-06CH11357. We thank to Professor Frederick R. Manby for stimulating discussions.

* Corresponding Author: esim@yonsei.ac.kr

[1] J. Maassen, W. Ji, and H. Guo, "Graphene spintronics: The role of ferromagnetic electrodes," Nano Letters, **11**, 151 (2011).

[2] I. Beljakov, V. Meded, F. Symalla, K. Fink, S. Shallcross, M. Ruben, and W. Wenzel, "Spin-crossover and massive anisotropy switching of 5d transition metal atoms on graphene nanoflakes," Nano Letters, **14**, 3364 (2014).

[3] A. Pronschinske, Y. Chen, G. F. Lewis, D. A. Shultz, A. Calzolari, M. Buongiorno Nardelli, and D. B. Dougherty, "Modification of molecular spin crossover in ultrathin films," Nano Letters, **13**, 1429 (2013).

[4] A. C. Aragons, D. Aravena, J. I. Cerd, Z. Acs-Castillo, H. Li, J. A. Real, F. Sanz, J. Hihath, E. Ruiz, and I. Dez-Prez, "Large conductance switching in a single-molecule device through room temperature spin-dependent transport," Nano Letters, **16**, 218 (2016).

[5] P. Zhou, C. Q. Sun, and L. Z. Sun, "Two dimensional antiferromagnetic chern insulator: Nirucl6," Nano Letters, **16**, 6325 (2016).

[6] X. Liu, J. Liu, L. Y. Antipina, J. Hu, C. Yue, A. M. Sanchez, P. B. Sorokin, Z. Mao, and J. Wei, "Direct fabrication of functional ultrathin single-crystal nanowires from quasi-one-dimensional van der waals crystals," Nano Letters, **16**, 6188 (2016).

[7] R. Frisenda, G. D. Harzmann, J. A. Celis Gil, J. M. Thijssen, M. Mayor, and H. S. J. van der Zant, "Stretching-induced conductance increase in a spin-crossover molecule," Nano Letters, **16**, 4733 (2016).

[8] R. Gaudenzi, E. Burzur, D. Reta, I. d. P. R. Moreira, S. T. Bromley, C. Rovira, J. Veciana, and H. S. J. van der Zant, "Exchange coupling inversion in a high-spin organic triradical molecule," Nano Letters, **16**, 2066 (2016).

[9] J. P. Perdew, M. Ernzerhof, K. Burke, and A. Savin, "On-top pair-density interpretation of spin density functional theory, with applications to magnetism," International Journal of Quantum Chemistry, **61**, 197 (1997).

[10] J. Harvey, "Dft computation of relative spin-state energetics of transition metal compounds," Principles and applications of density functional theory in inorganic chemistry I, 81 (2004).

[11] J. N. Harvey, "On the accuracy of density functional theory in transition metal chemistry," Annual Reports Section" C"(Physical Chemistry), **102**, 203 (2006).

[12] K. P. Kepp, "Consistent descriptions of metal–ligand bonds and spin-crossover in inorganic chemistry," Coordination Chemistry Reviews, **257**, 196 (2013).

[13] C. Toher, A. Filippetti, S. Sanvito, and K. Burke, "Self-interaction errors in density-functional calculations of electronic transport," Phys. Rev. Lett., **95**, 146402 (2005).

[14] S. Y. Quek, L. Venkataraman, H. J. Choi, S. G. Louie, M. S. Hybertsen, and J. B. Neaton, "Aminegold linked single-molecule circuits: experiment and theory," Nano Letters, **7**, 3477 (2007), pMID: 17900162.

[15] K. Burke, J. C. Angulo, and J. P. Perdew, "Validity of the extended electron-electron cusp condition," Physical Review A, **50**, 297 (1994).

[16] E. Ruiz, "Charge transport properties of spin crossover systems," Physical Chemistry Chemical Physics, **16**, 14 (2014).

[17] M. Reiher, O. Salomon, and B. Artur Hess, "Reparameterization of hybrid functionals based on energy differences of states of different multiplicity," Theoretical Chemistry Accounts, **107**, 48 (2001).

[18] C. Lefter, V. Davesne, L. Salmon, G. Molnar, P. Demont, A. Rotaru, and A. Bousseksou, "Charge transport and electrical properties of spin crossover materials: Towards nanoelectronic and spintronic devices," Magnetochemistry, **2**, 18 (2016).

[19] H. Paulsen and A. X. Trautwein, "Density functional theory calculations for spin crossover complexes," in *Spin Crossover in Transition Metal Compounds III* (Springer Berlin Heidelberg, Berlin, Heidelberg, 2004) pp. 197–219, ISBN 978-3-540-44984-3.

[20] M. Reiher, "Theoretical study of the fe (phen) 2 (ncs) 2 spin-crossover complex with reparametrized density functionals," Inorganic Chemistry, **41**, 6928 (2002).

[21] G. Ganzenmller, N. Berkane, A. Fouqueau, M. E. Casida, and M. Reiher, "Comparison of density functionals for differences between the high- (t2g5) and low- (a1g1) spin states of iron(ii) compounds. iv. results for the ferrous complexes [fe(l)(nhs4)]," The Journal of Chemical Physics, **122**, 234321 (2005).

[22] K. Pierloot and S. Vancoillie, "Relative energy of the high-(t2g5) and low-(a1g1) spin states of the ferrous complexes [fe(l)(nhs4)]: Caspt2 versus density functional theory," The Journal of Chemical Physics, **128**, 034104 (2008).

[23] T. Z. Gani and H. J. Kulik, "Where does the density localize? convergent behavior for global hybrids, range separation, and dft+ u," Journal of Chemical Theory and Computation, **12**, 5931 (2016).

[24] E. I. Ioannidis and H. J. Kulik, "Ligand-field-dependent behavior of meta-gga exchange in transition-metal complex spin-state ordering," The Journal of Physical Chemistry A, **121**, 874 (2017).

[25] P. Gütlich, A. Hauser, and H. Spiering, "Thermal and optical switching of iron (ii) complexes," Angewandte Chemie International Edition in English, **33**, 2024 (1994).

[26] M. Reiher, "A theoretical challenge: Transition-metal compounds," CHIMIA International Journal for Chemistry, **63**, 140 (2009).

[27] S. Ye and F. Neese, "Accurate modeling of spin-state energetics in spin-crossover systems with modern density functional theory," Inorganic Chemistry, **49**, 772 (2010).

[28] V. Meded, A. Bagrets, K. Fink, R. Chandrasekar, M. Ruben, F. Evers, A. Bernand-Mantel, J. S. Seldenthuis, A. Beukman, and H. S. J. van der Zant, "Electrical control over the fe(ii) spin crossover in a single molecule: Theory and experiment," Physical Review B, **83**, 245415 (2011).

[29] S. F. Matar, P. Guionneau, and G. Chastanet, "Multiscale experimental and theoretical investigations of spin crossover feii complexes: Examples of [fe(phen)2(ncs)2] and [fe(pmbia)2(ncs)2]," International Journal of Molecular Sciences, **16**, 4007 (2015).

[30] A. Fouqueau, S. Mer, M. E. Casida, L. M. Lawson Daku, A. Hauser, T. Mineva, and F. Neese, "Comparison of density functionals for energy and structural differences between the high- [5t2g:(t2g)4(eg)2] and low- [1a1g:(t2g)6(eg)0] spin states of the hexaquoferrous cation [fe(h2o)6]2+," The Journal of Chemical Physics, **120**, 9473 (2004).

[31] A. Fouqueau, M. E. Casida, L. M. L. Daku, A. Hauser, and F. Neese, "Comparison of density functionals for energy and structural differences between the high- [5t2g:(t2g)4(eg)2]

and low- [1a1g:(t2g)6(eg)0] spin states of iron(ii) coordination compounds. ii. more functionals and the hexaminoferrous cation, [fe(nh3)6]2+," The Journal of Chemical Physics, **122**, 044110 (2005).
[32] A. Droghetti, D. Alfè, and S. Sanvito, "Assessment of density functional theory for iron (ii) molecules across the spin-crossover transition," The Journal of Chemical Physics, **137**, 124303 (2012).
[33] L. M. Lawson Daku, F. Aquilante, T. W. Robinson, and A. Hauser, "Accurate spin-state energetics of transition metal complexes. 1. ccsd (t), caspt2, and dft study of [m (nch) 6] 2+(m= fe, co)," Journal of Chemical Theory and Computation, **8**, 4216 (2012).
[34] M. Radon, E. Broclawik, and K. Pierloot, "Electronic structure of selected {FeNO} 7 complexes in heme and non-heme architectures: A density functional and multireference ab initio study," The Journal of Physical Chemistry B, **114**, 1518 (2010).
[35] F. Furche and J. P. Perdew, "The performance of semilocal and hybrid density functionals in 3d transition-metal chemistry," The Journal of Chemical Physics, **124**, 044103 (2006).
[36] A. Droghetti, D. Alfè, and S. Sanvito, "Ground state of a spin-crossover molecule calculated by diffusion monte carlo," Phys. Rev. B, **87**, 205114 (2013).
[37] M.-C. Kim, E. Sim, and K. Burke, "Communication: Avoiding unbound anions in density functional calculations," The Journal of Chemical Physics, **134**, 171103 (2011).
[38] M.-C. Kim, E. Sim, and K. Burke, "Understanding and reducing errors in density functional calculations," Physical Review Letters, **111**, 073003 (2013).
[39] M.-C. Kim, E. Sim, and K. Burke, "Ions in solution: Density corrected density functional theory (dc-dft)," The Journal of Chemical Physics, **140**, 18A528 (2014).
[40] M.-C. Kim, H. Park, S. Son, E. Sim, and K. Burke, "Improved dft potential energy surfaces via improved densities," The Journal of Physical Chemistry Letters, **6**, 3802 (2015).
[41] A. Wasserman, J. Nafziger, K. Jiang, M.-C. Kim, E. Sim, and K. Burke, "The importance of being self-consistent," Annual Review of Physical Chemistry, **68**, 555 (2017).
[42] "TURBOMOLE V7.0 2015, a development of University of Karlsruhe and Forschungszentrum Karlsruhe GmbH, 1989-2007, TURBOMOLE GmbH, since 2007; available from `http://www.turbomole.com`." .
[43] C. L. Janssen and I. M. Nielsen, "New diagnostics for coupled-cluster and mllerplesset perturbation theory," Chemical Physics Letters, **290**, 423 (1998).
[44] J. Paldus and X. Li, "A critical assessment of the coupled cluster method in quantum chemistry," Advances in Chemical Physics, **110**, 1 (1999).
[45] W. M. Foulkes, L. Mitas, R. J. Needs, and G. Rajagopal, "Quantum Monte Carlo simulations of solids," Reviews of Modern Physics, **73**, 33 (2001).
[46] L. Shulenburger and T. R. Mattsson, "Quantum Monte Carlo applied to solids," Physical Review B, **88**, 1 (2013).
[47] J. A. Santana, J. T. Krogel, P. R. C. Kent, and F. A. Reboredo, "Cohesive energy and structural parameters of binary oxides of groups IIA and IIIB from diffusion quantum Monte Carlo," The Journal of Chemical Physics, **144**, 174707 (2016).
[48] J. T. Krogel, J. A. Santana, and F. A. Reboredo, "Pseudopotentials for quantum Monte Carlo studies of transition metal oxides," Physical Review B, **93**, 075143 (2016).
[49] H. Zheng and L. K. Wagner, "Computation of the correlated metal-insulator transition in vanadium dioxide from first principles." Physical Review Letters, **114**, 176401 (2015).
[50] J. A. Schiller, L. K. Wagner, and E. Ertekin, "Phase stability and properties of manganese oxide polymorphs: Assessment and insights from diffusion Monte Carlo," Physical Review B, **92**, 235209 (2015).
[51] F. R. Petruzielo, J. Toulouse, and C. J. Umrigar, "Approaching chemical accuracy with quantum Monte Carlo." The Journal of Chemical Physics, **136**, 124116 (2012).
[52] A. Benali, L. Shulenburger, N. A. Romero, J. Kim, and O. A. von Lilienfeld, "Application of diffusion monte carlo to materials dominated by van der waals interactions," Journal of Chemical Theory and Computation, **10**, 3417 (2014).
[53] M. Dubecky, P. Jurecka, R. Derian, P. Hobza, M. Otyepka, and L. Mitas, "Quantum Monte Carlo Methods Describe Noncovalent Interactions with Subchemical Accuracy," Journal of Chemical Theory and Computation, **9**, 4287 (2013).
[54] M. Dubecky, R. Derian, P. Jurecka, L. Mitas, P. Hobza, and M. Otyepka, "Quantum Monte Carlo for Noncovalent Interactions: An Efficient Protocol Attaining Benchmark Accuracy," Physical Chemistry Chemical Physics, **16**, 20915 (2014).
[55] L. Mitas, E. L. Shirley, and D. M. Ceperley, "Nonlocal pseudopotentials and diffusion Monte Carlo," Journal of Chemical Physics, **95**, 3467 (1991).
[56] A. Scemama, T. Applencourt, E. Giner, and M. Caffarel, "Accurate nonrelativistic ground-state energies of 3d transition metal atoms," The Journal of Chemical Physics, **141**, 244110 (2014).
[57] M. A. Morales, J. McMinis, B. K. Clark, J. Kim, and G. E. Scuseria, "Multideterminant wave functions in quantum monte carlo," Journal of Chemical Theory and Computation, **8**, 2181 (2012).
[58] L. K. Wagner and D. M. Ceperley, "Discovering correlated fermions using quantum monte carlo," Reports on Progress in Physics, **79**, 094501 (2016).
[59] K. Doblhoff-Dier, J. Meyer, P. E. Hoggan, G.-J. Kroes, and L. K. Wagner, "Diffusion monte carlo for accurate dissociation energies of 3d transition metal containing molecules," Journal of Chemical Theory and Computation, **12**, 2583 (2016), pMID: 27175914.
[60] A. Benali, L. Shulenburger, J. T. Krogel, X. Zhong, P. R. C. Kent, and O. Heinonen, "Quantum monte carlo analysis of a charge ordered insulating antiferromagnet: the ti4o7 magneli phase," Physical Chemistry Chemical Physics, **18**, 18323 (2016).
[61] Y. Luo, A. Benali, L. Shulenburger, J. T. Krogel, O. Heinonen, and P. R. C. Kent, "Phase stability of tio 2 polymorphs from diffusion quantum monte carlo," New Journal of Physics, **18**, 113049 (2016).
[62] J. A. Santana, J. T. Krogel, J. Kim, P. R. C. Kent, and F. A. Reboredo, "Structural stability and defect energetics of zno from diffusion quantum monte carlo," The Journal of Chemical Physics, **142**, 164705 (2015).
[63] L. K. Wagner, "Ground state of doped cuprates from first-principles quantum monte carlo calculations," Physical Review B, **92**, 161116 (2015).
[64] M. Caffarel, T. Applencourt, E. Giner, and A. Scemama, "Communication: Toward an improved control of the fixed-node error in quantum monte carlo: The case of the water molecule," The Journal of Chemical Physics, **144**, 151103 (2016).
[65] G. H. Booth, A. Gruneis, G. Kresse, and A. Alavi, "To-

wards an exact description of electronic wavefunctions in real solids," Nature, **493**, 365 (2013).
[66] T. Tsatsoulis, F. Hummel, D. Usvyat, M. Schütz, G. H. Booth, S. S. Binnie, M. J. Gillan, D. Alfè, A. Michaelides, and A. Grüneis, "A comparison between quantum chemistry and quantum monte carlo techniques for the adsorption of water on the (001) lih surface," The Journal of Chemical Physics, **146**, 204108 (2017).
[67] J. Kim, K. P. Esler, J. McMinis, M. A. Morales, B. K. Clark, L. Shulenburger, and D. M. Ceperley, "Hybrid algorithms in quantum monte carlo," Journal of Physics: Conference Series, **402**, 012008 (2012).
[68] J. Kim, K. Esler, J. McMinis, and D. M. Ceperley, in *Proceedings of the 2010 Scientific Discovery through Advanced Computing Conference* (2010).
[69] A. Mathuriya, Y. Luo, A. Benali, L. Shulenburger, and J. Kim, "Optimization and parallelization of b-spline based orbital evaluations in qmc on multi/many-core shared memory processors," arXiv preprint arXiv:1611.02665 (2016).
[70] L. Mitáš, "Quantum monte carlo calculation of the fe atom," Physical Review A, **49**, 4411 (1994).
[71] W. Kohn and L. J. Sham, "Self-consistent equations including exchange and correlation effects," Physical Review, **140**, A1133 (1965).
[72] J. P. Perdew, "Climbing the ladder of density functional approximations," MRS Bulletin, **38**, 743 (2013).
[73] A. J. Cohen, P. Mori-Sánchez, and W. Yang, "Insights into current limitations of density functional theory," Science, **321**, 792 (2008).
[74] P. Verma, A. Perera, and R. J. Bartlett, "Increasing the applicability of dft i: Non-variational correlation corrections from hartree–fock dft for predicting transition states," Chemical Physics Letters, **524**, 10 (2012).
[75] A. D. Becke, "Density-functional thermochemistry. iii. the role of exact exchange," The Journal of Chemical Physics, **98**, 5648 (1993).
[76] E. Giner, A. Scemama, and M. Caffarel, "Using perturbatively selected configuration interaction in quantum monte carlo calculations," Canadian Journal of Chemistry, **91**, 879 (2013).
[77] K. Boguslawski, C. R. Jacob, and M. Reiher, "Can dft accurately predict spin densities? analysis of discrepancies in iron nitrosyl complexes," Journal of Chemical Theory and Computation, **7**, 2740 (2011).
[78] K. Boguslawski, K. H. Marti, O. Legeza, and M. Reiher, "Accurate ab initio spin densities," Journal of Chemical Theory and Computation, **8**, 1970 (2012).
[79] http://tccl.yonsei.ac.kr/mediawiki/index.php/DC-DFT.
[80] V. Blum, M. Scheffler, R. Gehrke, F. Hanke, P. Havu, V. Havu, X. Ren, K. Reuter, and M. Scheffler, "The fritz haber institute ab initio molecular simulations package (fhi-aims)," http://www.fhi-berlin.mpg.de/aims (2009).
[81] C. Ning, B. Hajgató, Y. Huang, S. Zhang, K. Liu, Z. Luo, S. Knippenberg, J. Deng, and M. Deleuze, "High resolution electron momentum spectroscopy of the valence orbitals of water," Chemical Physics, **343**, 19 (2008).
[82] T. H. Dunning Jr, "Gaussian basis sets for use in correlated molecular calculations. i. the atoms boron through neon and hydrogen," The Journal of Chemical Physics, **90**, 1007 (1989).
[83] N. B. Balabanov and K. A. Peterson, "Systematically convergent basis sets for transition metals. i. all-electron correlation consistent basis sets for the 3 d elements sc–zn," The Journal of Chemical Physics, **123**, 064107 (2005).
[84] O. Treutler and R. Ahlrichs, "Efficient molecular numerical integration schemes," The Journal of Chemical Physics, **102**, 346 (1995).
[85] M. W. Schmidt, K. K. Baldridge, J. A. Boatz, S. T. Elbert, M. S. Gordon, J. H. Jensen, S. Koseki, N. Matsunaga, K. A. Nguyen, S. Su, T. L. Windus, M. Dupuis, and J. A. Montgomery, "General atomic and molecular electronic structure system," Journal of Computational Chemistry, **14**, 1347 (1993).
[86] C. Dykstra, G. Frenking, K. Kim, and G. Scuseria, *Theory and Applications of Computational Chemistry: the first forty years* (Elsevier, 2011).
[87] M. Burkatzki, C. Filippi, and M. Dolg, "Energy-consistent pseudopotentials for quantum monte carlo calculations," The Journal of Chemical Physics, **126**, 234105 (2007).
[88] M. Burkatzki, C. Filippi, and M. Dolg, "Energy-consistent small-core pseudopotentials for 3 d-transition metals adapted to quantum monte carlo calculations," The Journal of Chemical Physics, **129**, 164115 (2008).
[89] P. Stephens, F. Devlin, C. Chabalowski, and M. J. Frisch, "Ab initio calculation of vibrational absorption and circular dichroism spectra using density functional force fields," The Journal of Physical Chemistry, **98**, 11623 (1994).
[90] J. P. Perdew and A. Zunger, "Self-interaction correction to density-functional approximations for many-electron systems," Physical Review B, **23**, 5048 (1981).
[91] "available at https://aimsclub.fhi-berlin.mpg.de." .

## SUPPORTING INFORMATION

All HF, DFT, HF-DFT, and CCSD(T) calculations were carried out with TURBOMOLE v7.0.2.[42] We used the LDA, GGA (PBE, BP86, BLYP), mGGA (TPSS), Hybrid (TPSSh, B3LYP, PBE0, HH) functions to investigate the functional dependency across the various stages of "Jacob's ladder".[72] When optimizing the structure using LDA, GGA, and mGGA functions, it has well-known energetic issues, such as the LS over-stabilization and/or the over-binding molecular bonding.[12, 32] For instance, in the HS spin state of octahedral geometry, it is experimentally well known that an axial metal-ligand bond distance is 10-20% larger than that of an equatorial bond, but GGA often predicts all metal-ligand bonds to be equivalent. Such a characteristics is, in fact, a representative feature of the LS structure. Therefore, for each spin state of the $[Fe(L)_6]^{2+}$ complex, we used the optimized structure using B3LYP, regardless of the method used for energy calculations. In order to reduce the self-interaction error while maintaining the DFT level of computational efficiency, the corrected density was obtained from the HF calculation and the improved HF-DFT energy was obtained by applying the HF density to the approximate density functional. HF often results in a poor density when small basis set is used,[81] thus, we employed cc-pVTZ basis set[82, 83] for all HF, DFT, HF-DFT, and CCSD(T) calculations. For all HF and DFT cacula-tion, we adopted $10^{-8}$ self-consistent energy and $10^{-6}$ for one-electron density matrix convergence criteria. Lebedev's spherical grid integration was used for the DFT spherical integration and gridsize 6, i.e. 974 gridpoints were used. Multipole accelerated RI-J was used for the fast evaluation of the Coulomb potential.[84] All calculations on open-shell complexes were performed in $C_1$ symmetry.

We found agreement for self-consistent DFT and HF to within less than 0.1 eV on all SA energies when cc-pVTZ basis was used in TURBOMOLE and compared with the "really tight" default basis set and mesh in FHI-aims. The HF and PBE densities in Fig. 3 were generated using the default "really tight" setting for meshes and basis sets. Total electronic densities were collected from these calculations for comparison with DMC and GAMESS densities on a 10 Å$^3$ Cartesian grid with a spacing of 0.1 Å along the $x$-$y$, and $z$-directions.

A three-body Jastrow function reduced significantly the variance of the systems, and its parameters were carefully converged within variational MC. Both HF and DFT $\Psi_{AS}$ were used. They were generated and converged using the GAMESS package[85, 86] with a Gaussian basis set and an Effective Core Potential (ECP) developed specifically for many-body theory by Burkatzki, Filippi and Dolg[87, 88]. The ECP introduces errors below the FN-DMC error bar while reducing significantly the computation time. For each atom, we use the basis set for which the ECP was developed: ANO-ccpVTZ[88] for Fe and a cc-pVTZ[87] for the remaining atoms, respectively. (Increasing to quintuple zeta produced changes smaller than the error bars of FN-DMC, confirming previous observations of weak basis-set dependence. Initial $\Psi_{AS}$(DFT) wavefunctions were generated using B3LYP[75, 89], as its energies were about 0.13±0.03 eV below those from LDA wavefunction[90]. To reach a statistical error bar below 0.03 eV per molecule and to avoid any correlated sampling or population bias, we used 8192 walkers. A time step of 0.001 a.u. introduced negligible error.

TABLE S1. Raw data of $[Fe(L)_6]^{2+}$ where L is CO, and $H_2O$. HF-DFT indicates DC-DFT with HF density.[79]

| | CO | | $H_2O$ | |
|---|---|---|---|---|
| | HS | LS | HS | LS |
| AB INITIO | | | | |
| HF | -1938.596688 | -1938.425659 | -1718.487158 | -1718.355787 |
| CCSD | -1941.486969 | -1941.501497 | -1720.712183 | -1720.639633 |
| CCSD(T) | -1941.61279 | -1941.661758 | -1720.774355 | -1720.7099 |
| SC-DFT | | | | |
| SVWN | -1935.562476 | -1935.75007 | -1716.324658 | -1716.307699 |
| BP86 | -1943.524592 | -1943.645874 | -1722.303555 | -1722.263269 |
| BLYP | -1943.282952 | -1943.383951 | -1722.036727 | -1722.001664 |
| PBE | -1942.315225 | -1942.439855 | -1721.33526 | -1721.293755 |
| TPSS | -1943.431767 | -1943.544462 | -1722.135513 | -1722.101699 |
| TPSSh | -1943.318874 | -1943.401835 | -1722.071487 | -1722.027418 |
| B3LYP | -1942.918583 | -1942.965452 | -1721.807611 | -1721.755856 |
| PBE0 | -1942.307023 | -1942.356275 | -1721.373081 | -1721.308412 |
| HH | -1942.925932 | -1942.898408 | -1721.836892 | -1721.764887 |
| HF-DFT | | | | |
| SVWN(HF) | -1935.324969 | -1935.400057 | -1716.179002 | -1716.123761 |
| BP86(HF) | -1943.359619 | -1943.379374 | -1722.205822 | -1722.133963 |
| BLYP(HF) | -1943.098747 | -1943.108379 | -1721.922532 | -1721.861337 |
| PBE(HF) | -1942.149806 | -1942.169324 | -1721.240425 | -1721.166759 |
| TPSS(HF) | -1943.300547 | -1943.323445 | -1722.05761 | -1721.996494 |
| TPSSh(HF) | -1943.216065 | -1943.226898 | -1722.011766 | -1721.945904 |
| B3LYP(HF) | -1942.803829 | -1942.7941 | -1721.737777 | -1721.670029 |
| PBE0(HF) | -1942.221245 | -1942.212253 | -1721.326427 | -1721.244492 |
| HH(HF) | -1942.88147 | -1942.835129 | -1721.810121 | -1721.732972 |

TABLE S2. Raw data of $[Fe(L)_6]^{2+}$ where L is CO and $H_2O$. "aimsRT2" indicates FHI-aims[91] with the default "really tight" settings for basis set, mesh, and angular momentum expansion of the Hartree potential; "aimsRT3+2" indicates the "really tight" default setting for mesh and expansion of the Hartree potential and the Tier 3 basis set with added two Tier 4 basis functions for Fe (hydro 5 f 12 and hydro g 10.4). Relativistic corrections were turned off with the setting "override_relativity .true."

| | CO | | $H_2O$ | |
|---|---|---|---|---|
| | HS | LS | HS | LS |
| FHI-aims | | | | |
| HF(aimsRT2) | -1938.59753 | -1938.43178 | -1718.494936 | -1718.366256 |
| HF(aimsRT3+2) | -1938.63999 | -1938.46939 | -1718.520974 | -1718.391508 |
| B3LYP(aimsRT2) | -1943.40144 | -1943.44917 | -1722.185538 | -1722.13375 |
| B3LYP(aimsRT3+2) | -1943.406195 | -1943.453468 | -1722.188232 | -1722.136102 |
| GAMESS (cc-pVTZ) | | | | |
| HF(gam) | | -1938.589781 | -1938.425386 | |
| B3LYP(gam) | -1942.914743 | -1942.965171 | -1721.803708 | -1721.754757 |
| DMC | | | | |
| DMC(B3LYP) | -1943.323152 | -1943.344858 | -1722.234695 | -1722.169160 |
| Error | 0.000713 | 0.000669 | 0.000546 | 0.000598 |

TABLE S3. Raw data of $[Fe(L)_6]^{2+}$ where L is NCH and $NH_3$.

| | NCH | | $NH_3$ | |
|---|---|---|---|---|
| | HS | LS | HS | LS |
| | | AB INITIO | | |
| HF | -1819.620374 | -1819.487347 | -1599.491142 | -1599.371166 |
| CCSD | -1822.423771 | -1822.390926 | -1601.621124 | -1601.58094 |
| CCSD(T) | -1822.547794 | -1822.531749 | -1601.685784 | -1601.657385 |
| | | SC-DFT | | |
| SVWN | -1816.857548 | -1816.93601 | -1597.590343 | -1597.622558 |
| BP86 | -1824.320552 | -1824.353601 | -1603.094831 | -1603.095664 |
| BLYP | -1824.044252 | -1824.072593 | -1602.780882 | -1602.782754 |
| PBE | -1823.179736 | -1823.212964 | -1602.195969 | -1602.196691 |
| TPSS | -1824.237428 | -1824.271398 | -1602.943456 | -1602.948892 |
| TPSSh | -1824.142661 | -1824.15655 | -1602.892938 | -1602.884685 |
| B3LYP | -1823.74587 | -1823.739341 | -1602.608817 | -1602.58767 |
| PBE0 | -1823.202688 | -1823.187878 | -1602.255415 | -1602.224025 |
| HH | -1823.765913 | -1823.719894 | -1602.643047 | -1602.594119 |
| | | HF-DFT | | |
| SVWN(HF) | -1816.63952 | -1816.638734 | -1597.442603 | -1597.420226 |
| BP86(HF) | -1824.171878 | -1824.136674 | -1602.995131 | -1602.950198 |
| BLYP(HF) | -1823.875086 | -1823.842955 | -1602.665414 | -1602.62815 |
| PBE(HF) | -1823.032117 | -1822.995094 | -1602.099135 | -1602.052967 |
| TPSS(HF) | -1824.121705 | -1824.09658 | -1602.865679 | -1602.831769 |
| TPSSh(HF) | -1824.051686 | -1824.02009 | -1602.832908 | -1602.793536 |
| B3LYP(HF) | -1823.639404 | -1823.598725 | -1602.537834 | -1602.49317 |
| PBE0(HF) | -1823.125538 | -1823.076015 | -1602.206621 | -1602.150437 |
| HH(HF) | -1823.723703 | -1823.667414 | -1602.615548 | -1602.559095 |

TABLE S4. Raw data of $[Fe(L)_6]^{2+}$ where L is NCH and $NH_3$.

| | NCH | | $NH_3$ | |
|---|---|---|---|---|
| | HS | LS | HS | LS |
| | | GAMES/ECP | | |
| B3LYP(gam) | -1823.742016 | -1823.738646 | -1602.604559 | -1602.586481 |
| | | DMC | | |
| DMC(B3LYP) | -1824.201405 | -1824.158306 | -1603.025729 | -1602.980673 |
| Error | 0.000968 | 0.000738 | 0.000565 | 0.000773 |

TABLE S5. $[Fe(CO)_6]^{2+}$ xyz data.

| CO_HS | | | | CO_LS | | | |
|---|---|---|---|---|---|---|---|
| 13 | | | | 13 | | | |
| | | | | | | | |
| Fe | 0.0000013 | -0.0000001 | -0.0000001 | Fe | 0.0000002 | 0.0000002 | 0.0000001 |
| C | 0.0000037 | -0.0072194 | 2.3405884 | C | 0.0000001 | 0.0000002 | 1.9494602 |
| O | -0.0000299 | -0.0415619 | 3.4549199 | O | -0.0000002 | -0.0000001 | 3.0656647 |
| C | 2.3029923 | -0.0000137 | -0.0000135 | C | 1.9494601 | 0.0000000 | -0.0000001 |
| O | 3.4182461 | -0.0000170 | -0.0000168 | O | 3.0656646 | -0.0000003 | -0.0000005 |
| C | -2.3029877 | 0.0000133 | 0.0000131 | C | -1.9494597 | 0.0000000 | -0.0000001 |
| O | -3.4182415 | 0.0000167 | 0.0000165 | O | -3.0656642 | -0.0000003 | -0.0000005 |
| C | -0.0000019 | 0.0072196 | -2.3405883 | C | 0.0000001 | -0.0000001 | -1.9494600 |
| O | 0.0000250 | 0.0415622 | -3.4549197 | O | -0.0000003 | -0.0000004 | -3.0656645 |
| C | -0.0000028 | -2.3369861 | 0.0065791 | C | 0.0000000 | -1.9494597 | 0.0000002 |
| O | 0.0000240 | -3.4513475 | 0.0412328 | O | -0.0000003 | -3.0656642 | -0.0000001 |
| C | 0.0000037 | 2.3369862 | -0.0065788 | C | 0.0000000 | 1.9494600 | 0.0000001 |
| O | -0.0000326 | 3.4513476 | -0.0412324 | O | -0.0000003 | 3.0656646 | 0.0000004 |

TABLE S6. $[Fe(NCH)_6]^{2+}$ xyz data.

| NCH_HS | | | | NCH_LS | | | |
|---|---|---|---|---|---|---|---|
| 19 | | | | 19 | | | |
| | | | | | | | |
| Fe | 0.0000000 | 0.0000005 | -0.0000008 | Fe | 0.0000000 | 0.0000000 | 0.0000003 |
| N | 0.0000002 | 2.2062681 | -0.0000002 | N | 0.0000000 | 1.9756648 | 0.0000002 |
| N | -2.2009845 | 0.0000002 | -0.0000003 | N | -1.9756648 | 0.0000000 | 0.0000002 |
| N | -0.0000004 | -0.0000004 | -2.2009794 | N | -0.0000001 | 0.0000001 | -1.9756664 |
| N | -0.0000004 | -0.0000004 | 2.2009781 | N | 0.0000000 | 0.0000001 | 1.9756669 |
| N | 2.2009844 | 0.0000010 | -0.0000003 | N | 1.9756648 | -0.0000001 | 0.0000002 |
| N | 0.0000007 | -2.2062673 | -0.0000003 | N | 0.0000000 | -1.9756648 | 0.0000002 |
| C | 0.0000012 | -3.3493502 | 0.0000003 | C | 0.0000004 | -3.1177203 | -0.0000002 |
| H | 0.0000016 | -4.4237178 | 0.0000007 | H | 0.0000007 | -4.1914191 | -0.0000004 |
| C | -3.3446088 | 0.0000009 | 0.0000007 | C | -3.1177203 | -0.0000005 | -0.0000002 |
| H | -4.4184325 | 0.0000014 | 0.0000013 | H | -4.1914191 | -0.0000008 | -0.0000005 |
| C | -0.0000010 | -0.0000013 | -3.3446039 | C | -0.0000004 | 0.0000004 | -3.1177221 |
| H | -0.0000013 | -0.0000020 | -4.4184276 | H | -0.0000007 | 0.0000007 | -4.1914211 |
| C | 3.3446087 | 0.0000005 | 0.0000006 | C | 3.1177203 | -0.0000005 | -0.0000002 |
| H | 4.4184324 | 0.0000002 | 0.0000013 | H | 4.1914191 | -0.0000008 | -0.0000005 |
| C | -0.0000010 | -0.0000013 | 3.3446025 | C | -0.0000005 | 0.0000004 | 3.1177226 |
| H | -0.0000014 | -0.0000020 | 4.4184262 | H | -0.0000008 | 0.0000007 | 4.1914216 |
| C | 0.0000007 | 3.3493510 | 0.0000003 | C | 0.0000004 | 3.1177203 | -0.0000002 |
| H | 0.0000011 | 4.4237186 | 0.0000007 | H | 0.0000007 | 4.1914191 | -0.0000004 |

TABLE S7. $[Fe(NH_3)_6]^{2+}$ xyz data.

| NH3_HS | | | | NH3_LS | | | |
|---|---|---|---|---|---|---|---|
| 25 | | | | 25 | | | |
| | | | | | | | |
| Fe | -1.6827629 | -0.5620638 | 0.0006858 | Fe | -1.6825128 | -0.5610153 | -0.0006961 |
| N | -1.7654701 | 1.7386430 | -0.0155915 | N | -1.7424118 | 1.5552120 | 0.0158045 |
| H | -2.3091690 | 2.1062136 | 0.7643967 | H | -2.4036875 | 1.9339858 | 0.6938915 |
| H | -0.8575605 | 2.1961896 | 0.0569999 | H | -0.8559216 | 2.0036953 | 0.2471666 |
| H | -2.1985074 | 2.1444062 | -0.8446345 | H | -2.0193966 | 1.9820701 | -0.8682401 |
| N | 0.6370910 | -0.4829211 | 0.0198374 | N | 0.4336893 | -0.5015161 | 0.0181596 |
| H | 1.0410909 | -0.1381987 | 0.8898340 | H | 0.8440623 | -0.2468840 | 0.9166699 |
| H | 1.0933299 | -1.3794527 | -0.1444124 | H | 0.8887488 | -1.3803696 | -0.2288050 |
| H | 1.0148101 | 0.1305669 | -0.7014791 | H | 0.8222226 | 0.1746500 | -0.6393939 |
| N | -4.0024708 | -0.5711646 | -0.0821798 | N | -3.7986910 | -0.5778442 | -0.0617939 |
| H | -4.4120209 | -1.4547568 | -0.3829660 | H | -4.2102994 | -1.4780144 | -0.3084425 |
| H | -4.4588691 | -0.3582133 | 0.8039661 | H | -4.2539588 | -0.3220773 | 0.8144309 |
| H | -4.3743783 | 0.1202099 | -0.7325748 | H | -4.1858156 | 0.0740192 | -0.7442454 |
| N | -1.6769265 | -2.8574940 | 0.0683045 | N | -1.6610569 | -2.6779301 | 0.0242933 |
| H | -2.4248044 | -3.2491480 | 0.6399273 | H | -2.3903796 | -3.0814636 | 0.6123051 |
| H | -1.8046273 | -3.2785580 | -0.8511997 | H | -1.7968348 | -3.1174279 | -0.8861569 |
| H | -0.8224786 | -3.2773553 | 0.4326991 | H | -0.7980809 | -3.0901543 | 0.3789793 |
| N | -1.6947644 | -0.6233020 | 2.2950899 | N | -1.7053421 | -0.5825425 | 2.1162469 |
| H | -0.9567299 | -1.2059553 | 2.6891561 | H | -0.9813845 | -1.1763493 | 2.5209486 |
| H | -1.5535805 | 0.2946430 | 2.7152532 | H | -1.5616171 | 0.3273586 | 2.5543575 |
| H | -2.5558826 | -0.9737822 | 2.7131764 | H | -2.5715855 | -0.9289025 | 2.5286917 |
| N | -1.5929695 | -0.5620411 | -2.2999504 | N | -1.6210680 | -0.5813637 | -2.1168366 |
| H | -1.0185358 | -1.3236265 | -2.6592866 | H | -0.9545040 | -1.2553296 | -2.4936978 |
| H | -2.4963312 | -0.6738135 | -2.7585987 | H | -2.5055538 | -0.8204390 | -2.5652371 |
| H | -1.1916622 | 0.2796750 | -2.7122128 | H | -1.3505210 | 0.3037723 | -2.5455600 |

TABLE S8. $[Fe(H_2O)_6]^{2+}$ xyz data.

| H2O_HS | | | | H2O_LS | | | |
|---|---|---|---|---|---|---|---|
| 19 | | | | 19 | | | |
| | | | | | | | |
| Fe | -1.6845392 | -0.7206701 | -0.1386922 | Fe | -1.6845545 | -0.7208248 | -0.1387753 |
| O | -1.7225165 | 1.4435451 | -0.0788233 | O | -1.8371609 | 1.3103074 | -0.2366417 |
| H | -2.2327347 | 2.0721657 | -0.6081837 | H | -2.7248031 | 1.6951387 | -0.1781363 |
| H | -1.1836565 | 1.9689883 | 0.5299181 | H | -1.2260721 | 1.9506903 | 0.1550818 |
| O | 0.4742655 | -0.5541733 | -0.1258573 | O | 0.3478431 | -0.6860383 | 0.0239942 |
| H | 1.1321101 | -1.0258989 | 0.4036902 | H | 0.8167239 | -1.5311871 | -0.0487537 |
| H | 0.9645036 | 0.0562592 | -0.6951254 | H | 0.9394100 | -0.0045677 | -0.3261609 |
| O | -3.8432628 | -0.8879805 | -0.1526380 | O | -3.7191775 | -0.7293063 | -0.2749855 |
| H | -4.3335551 | -1.4967341 | 0.4183794 | H | -4.3343364 | -1.1264790 | 0.3580976 |
| H | -4.5012426 | -0.4156202 | -0.6814497 | H | -4.1078491 | -0.8432878 | -1.1555310 |
| O | -1.6468488 | -2.8848921 | -0.1975952 | O | -1.5049607 | -2.7508363 | -0.0662374 |
| H | -2.1866691 | -3.4101261 | -0.8056683 | H | -1.8213499 | -3.3785131 | -0.7317227 |
| H | -1.1337667 | -3.5136153 | 0.3288629 | H | -1.6098710 | -3.1783680 | 0.7972597 |
| O | -1.8336924 | -0.6522882 | 2.0203864 | O | -1.6955636 | -0.7997349 | 1.8988762 |
| H | -1.3324137 | -1.1313887 | 2.6948456 | H | -0.8512825 | -0.6664715 | 2.3558853 |
| H | -2.4655514 | -0.0913583 | 2.4927695 | H | -2.3885668 | -0.4582020 | 2.4820276 |
| O | -1.5352491 | -0.7884118 | -2.2977680 | O | -1.6983650 | -0.6692265 | -2.1773196 |
| H | -0.9010307 | -1.3468668 | -2.7699235 | H | -1.2754814 | -1.3071697 | -2.7698947 |
| H | -2.0404799 | -0.3138537 | -2.9724876 | H | -1.6308724 | 0.1989462 | -2.6029238 |

TABLE S9. $Fe^{2+}$ atomic charge of $[Fe(L)_6]^{2+}$ with various Metal-Ligand distance. DFT shows insufficient atomic charge due to the self-interaction error while HF does not.

| | RM-L | HF | PBE | LS | | HF | PBE |
|---|---|---|---|---|---|---|---|
| CO_HS | Req=2.3 | 1.08 | 0.57 | CO_LS | Req=1.9 | 0.33 | -0.39 |
| | Rinf=5.0 | 1.94 | 1.16 | | Rinf=5.0 | 1.93 | 1.05 |
| NCH_HS | Req=2.2 | 1.70 | 1.04 | NCH_LS | Req=2.0 | 1.37 | 0.56 |
| | Rinf=5.0 | 1.95 | 1.21 | | Rinf=5.0 | 1.95 | 1.13 |
| NH3_HS | Req=2.3 | 1.46 | 0.72 | NH3_LS | Req=2.1 | 1.32 | 0.28 |
| | | | | | Rinf=5.0 | | 0.76 |
| H2O_HS | Req=2.2 | 1.43 | 0.79 | H2O_LS | Req=2.0 | 1.31 | 0.51 |
| | Rinf=5.0 | 1.95 | 1.02 | | Rinf=5.0 | 1.94 | 0.92 |

TABLE S10. $[Fe(L)_6]^{2+}$ HOMO-LUMO gap of HF and PBE. Note that all units are eV.

| | HF | PBE |
|---|---|---|
| CO_HS | 15.33 | 0.45 |
| CO_LS | 17.99 | 3.98 |
| NCH_HS | 15.04 | 0.43 |
| NCH_LS | 16.38 | 2.44 |
| NH3_HS | 13.82 | 0.47 |
| NH3_LS | 15.40 | 1.91 |
| H2O_HS | 14.57 | 0.66 |
| H2O_LS | 16.25 | 1.38 |

TABLE S11. Raw data of $[Fe(L)_6]^{2+}$ where L is CO, and $H_2O$, TZVP basis set.

| | CO | | H2O | |
|---|---|---|---|---|
| | HS | LS | HS | LS |
| AB INITIO | | | | |
| HF | -1938.544195 | -1938.368443 | -1718.45312 | -1718.315537 |
| CCSD | -1940.931932 | -1940.919423 | -1720.182227 | -1720.098026 |
| CCSD(T) | -1941.026375 | -1941.038878 | -1720.220097 | -1720.141748 |
| SC-DFT | | | | |
| SVWN_TZVP | -1935.562476 | -1935.75007 | -1716.324658 | -1716.307699 |
| BP86_TZVP | -1943.490062 | -1943.609566 | -1722.272681 | -1722.230268 |
| BLYP_TZVP | -1943.245756 | -1943.345428 | -1722.004401 | -1721.967074 |
| PBE_TZVP | -1942.28028 | -1942.403351 | -1721.304821 | -1721.261134 |
| TPSS_TZVP | -1943.39643 | -1943.507391 | -1722.107634 | -1722.072356 |
| TPSSh_TZVP | -1943.282565 | -1943.36364 | -1722.043473 | -1721.998094 |
| B3LYP_TZVP | -1942.879188 | -1942.924235 | -1721.775629 | -1721.721931 |
| PBE0_TZVP | -1942.269433 | -1942.316757 | -1721.343075 | -1721.276812 |
| HH_TZVP | -1942.883119 | -1942.853297 | -1721.805249 | -1721.730594 |
| HF-DFT | | | | |
| SVWN(HF)_TZVP | -1935.299796 | -1935.378935 | -1716.15509 | -1716.105853 |
| BP86(HF)_TZVP | -1943.333361 | -1943.356739 | -1722.1811 | -1722.114554 |
| BLYP(HF)_TZVP | -1943.071378 | -1943.084017 | -1721.897645 | -1721.840542 |
| PBE(HF)_TZVP | -1942.122074 | -1942.145724 | -1721.215951 | -1721.147715 |
| TPSS(HF)_TZVP | -1943.270719 | -1943.296682 | -1722.034244 | -1721.977504 |
| TPSSh(HF)_TZVP | -1943.184032 | -1943.197198 | -1721.987336 | -1721.924908 |
| B3LYP(HF)_TZVP | -1942.771561 | -1942.763296 | -1721.711073 | -1721.645457 |
| PBE0(HF)_TZVP | -1942.187458 | -1942.180504 | -1721.299684 | -1721.220548 |
| HH(HF)_TZVP | -1942.841231 | -1942.79396 | -1721.780398 | -1721.702109 |

TABLE S12. Raw data of $[Fe(L)_6]^{2+}$ where L is NCH and $NH_3$, TZVP basis set.

| | NCH | | $NH_3$ | |
|---|---|---|---|---|
| | HS | LS | HS | LS |
| AB INITIO | | | | |
| HF | -1819.575158 | -1819.435748 | -1599.452665 | -1599.327687 |
| CCSD | -1821.896763 | -1821.846661 | -1601.123217 | -1601.069463 |
| CCSD(T) | -1821.990379 | -1821.952622 | -1601.165067 | -1601.119688 |
| SC-DFT | | | | |
| SVWN_TZVP | -1816.857548 | -1816.93601 | -1597.590343 | -1597.622558 |
| BP86_TZVP | -1824.284226 | -1824.315432 | -1603.057978 | -1603.056034 |
| BLYP_TZVP | -1824.005452 | -1824.032018 | -1602.741823 | -1602.741127 |
| PBE_TZVP | -1823.14398 | -1823.175345 | -1602.159974 | -1602.157843 |
| TPSS_TZVP | -1824.201308 | -1824.234426 | -1602.909479 | -1602.913085 |
| TPSSh_TZVP | -1824.106194 | -1824.119101 | -1602.85921 | -1602.849486 |
| B3LYP_TZVP | -1823.706825 | -1823.698327 | -1602.571109 | -1602.548127 |
| PBE0_TZVP | -1823.166204 | -1823.149511 | -1602.2208 | -1602.187785 |
| HH_TZVP | -1823.726392 | -1823.67743 | -1602.606373 | -1602.555522 |
| HF-DFT | | | | |
| SVWN(HF)_TZVP | -1816.613916 | -1816.618223 | -1597.415187 | -1597.399208 |
| BP86(HF)_TZVP | -1824.143582 | -1824.112787 | -1602.966054 | -1602.926874 |
| BLYP(HF)_TZVP | -1823.846515 | -1823.817712 | -1602.635138 | -1602.602517 |
| PBE(HF)_TZVP | -1823.003816 | -1822.971334 | -1602.070621 | -1602.03038 |
| TPSS(HF)_TZVP | -1824.090705 | -1824.069565 | -1602.83662 | -1602.80771 |
| TPSSh(HF)_TZVP | -1824.019271 | -1823.990722 | -1602.80304 | -1602.767774 |
| B3LYP(HF)_TZVP | -1823.607715 | -1823.568499 | -1602.50611 | -1602.464246 |
| PBE0(HF)_TZVP | -1823.093083 | -1823.045631 | -1602.176074 | -1602.123345 |
| HH(HF)_TZVP | -1823.687019 | -1823.629106 | -1602.5811 | -1602.524398 |

TABLE S13. Raw data of $[Fe(L)_6]^{2+}$, cc-pVDZ basis where L is CO, $H_2O$, NCH and $NH_3$

| | cc-pVDZ | |
|---|---|---|
| | CCSD(T) | CCSD |
| CO_HS | -1940.683472 | -1940.601943 |
| CO_LS | -1940.718958 | -1940.608786 |
| H2O_HS | -1720.005539 | -1719.974971 |
| H2O_LS | -1719.933587 | -1719.896417 |
| NCH_HS | -1821.683798 | -1821.600966 |
| NCH_LS | -1821.655531 | -1821.559138 |
| NH3_HS | -1601.02068 | -1600.983348 |
| NH3_LS | -1600.984901 | -1600.937788 |

TABLE S14. $[Fe(L)_6]^{2+}$ D1 diagnostics (CCSD) of cc-pVDZ, cc-pVTZ and TZVP basis sets.

| | cc-pVDZ | cc-pVTZ | TZVP |
|---|---|---|---|
| CO_HS | 0.0598 | 0.0602 | 0.0538 |
| CO_LS | 0.1419 | 0.1438 | 0.1305 |
| H2O_HS | 0.0374 | 0.0381 | 0.0339 |
| H2O_LS | 0.059 | 0.0604 | 0.0536 |
| NCH_HS | 0.0591 | 0.0508 | 0.0503 |
| NCH_LS | 0.0866 | 0.0874 | 0.0853 |
| NH3_HS | 0.0562 | 0.0575 | 0.0494 |
| NH3_LS | 0.0865 | 0.0872 | 0.076 |

## LIST OF FIGURES



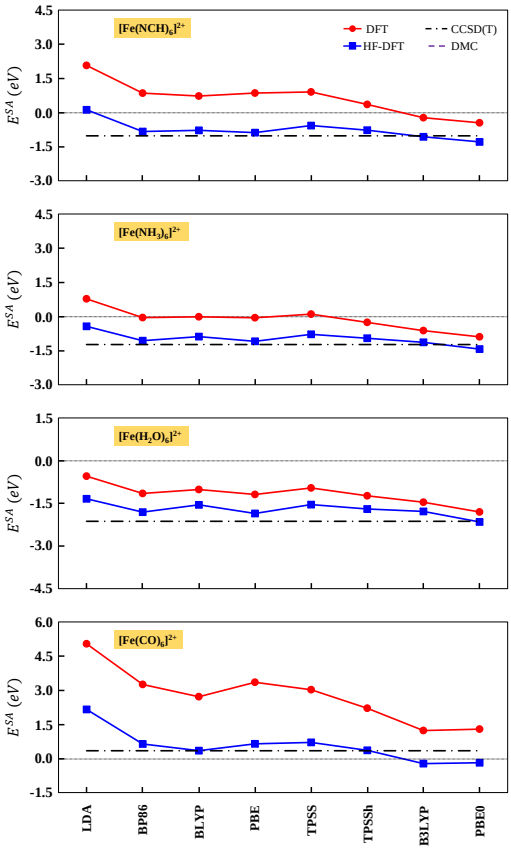


FIG. S1. Spin adiabatic energy differences in eV of Fe complexes for various DFT calculations and CCSD(T). All DFT and HF-DFT used TZVP basis set.

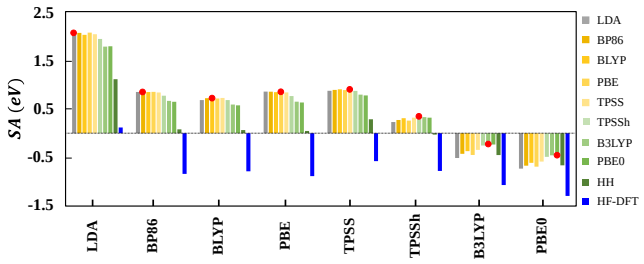


FIG. S2. SA rainbow plot of NCH complex evaluated with several different XC approximations on different self-consistent densities (red dots) and the HF density (blue bar) using TZVP basis set. The x-axis labels the energy functional, the colored bars indicate which density (grey is LDA, yellow is GGA/mGGA, green is hybrid, and blue is HF). The dark green bar uses the self-consistent density of Becke's half-and-half functional (HH), which contains 50% exact exchange.

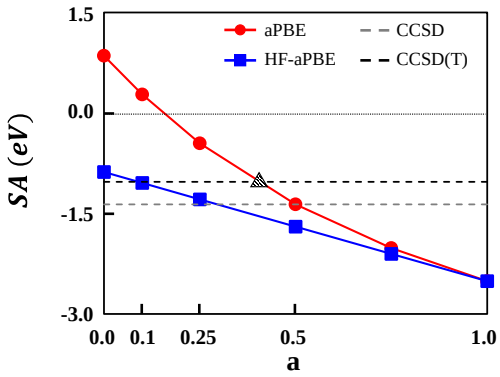


FIG. S3. $a$PBE and HF-$a$PBE of $[Fe(NCH)_6]^{2+}$, TZVP basis set.